Regenerative Therapy 26 (2024) 188–202

Contents lists available at ScienceDirect

Regenerative Therapy

journal homepage: http://www.elsevier.com/locate/reth

Original Article

# Alpha terpineol preconditioning enhances regenerative potential of mesenchymal stem cells in full thickness acid burn wounds

Fatima Jameel [a], Fatima Irfan [a], Asmat Salim [a, *], Irfan Khan [a], Enam A. Khalil [b]

[a] Stem Cell Research Laboratory, Dr. Panjwani Center for Molecular Medicine and Drug Research, International Center for Chemical and Biological Sciences, University of Karachi, Karachi, 75270, Pakistan
[b] Department of Pharmacy, The University of Jordan, Amman, 11942, Jordan

ARTICLE INFO

*Article history:*
Received 7 March 2024
Received in revised form
6 May 2024
Accepted 19 May 2024

*Keywords:*
Acid burn wounds
Alpha terpineol
Preconditioning
Mesenchymal stem cells
Wound healing

ABSTRACT

Regeneration of full thickness burn wounds is a significant clinical challenge. Direct stem cell transplantation at the wound site has a promising effect on wound regeneration. However, stem cell survival within the harsh wound environment is critically compromised. In this regard, preconditioning of stem cells with cytoprotective compounds can improve the efficiency of transplanted cells. This study evaluated the possible effect of alpha terpineol (αT) preconditioned mesenchymal stem cells (αT-MSCs) in full thickness acid burn wound. An optimized concentration of 10 μM αT was used for MSC preconditioning, followed by scratch assay analysis. A novel rat model of full thickness acid burn wound was developed and characterized *via* macroscopic and histological examinations. Treatment (normal and αT-MSCs) was given after 48 h of burn wound induction, and the healing pattern was examined till day 40. Skin tissues were harvested at the early (day 10) and late (day 40) wound healing phases and examined by histological grading, neovascularization, and gene expression profiling of healing mediators. In scratch assay, αT-MSCs exhibited enhanced cell migration and wound closure (scratch gap) compared to normal MSCs. *In vivo* findings revealed enhanced regeneration in the wound treated with αT-MSCs compared to normal MSCs and untreated control. Histology revealed enhanced collagen deposition with regenerated skin layers in normal MSC- and αT-MSC treated groups compared to the untreated control. These findings were correlated with enhanced expression of α-SMA as shown by immunohistochemistry. Additionally, αT-MSC group showed reduced inflammation and oxidative stress, and enhanced regeneration, as witnessed by a decrease in *IL-1β*, *IL-6*, *TNF-α*, and *Bax* and an increase in *BCL-2, PRDX-4, GPX-7, SOD-1*, *VEGF*, *EGF*, *FGF*, *MMP-9*, *PDGF*, and *TGF-β* gene expression levels at early and late phases, respectively. Overall findings demonstrated that αT exerts its therapeutic effect by mitigating excessive inflammation and oxidative stress while concurrently enhancing neovascularization. Thus, this study offers new perspectives on managing full thickness acid burn wounds in future clinical settings.


## 1. Introduction

Burn wounds represent devastating tissue injuries necessitating immediate medical attention. Different chemicals used in industries and households may cause skin burns and elicit severe systemic effects after inhalation or absorption [1]. The disability due to chemical burns depends upon the nature of the injury, either accidental or deliberate exposure. Causative agents for chemical injuries vary in geographical location and industrial settings. It has been estimated from epidemiological studies that over 25,000 chemicals that are frequently used in homes, agriculture, and industries possess the potential for burn injury [2]. It is consistently reported that chemical injuries due to acid exposure cause skin damage by denaturing and precipitating proteins in the tissues [3,4].

For the past few years, acid burns have been associated with domestic violence, mostly in women, resulting in permanent

* Corresponding author. Dr. Panjwani Center for Molecular Medicine and Drug Research, International Center for Chemical and Biological Sciences, University of Karachi, Karachi, 75270, Pakistan.
*E-mail address:* asmat.salim@iccs.edu (A. Salim).
Peer review under responsibility of the Japanese Society for Regenerative Medicine.

https://doi.org/10.1016/j.reth.2024.05.008

disfigurement. However, many cases of acid assaults are not even reported due to socially sensitive matters [5]. Pathophysiological studies on acid burns reveal the destruction of all layers of skin, protein denaturation, necrosis, ischemia, blisters, eschar, and vascular damage [6,7]. These injuries cause a prolonged effect on the body, resulting in long-term dependency and compromised body functions. To repair the compromised function of wound tissues, the skin initiates a wound healing cascade that starts with inflammation and ends with restoration in between a proliferative phase [8]. However, this healing cascade is affected by extensive oxidative stress, inflammation, wound infection, and uncontrolled fibrosis, which ultimately cause hypertrophic scars and the inability to restore the damaged tissue [9,10].

Treatment options are available globally, but their therapeutic effects are not sufficiently potent for extensive burn wounds. The efficacy of the therapeutics mainly depends on the early wound excision followed by repetitive wound dressings and plastic surgeries [5]. Autologous skin grafts are widely used for burn treatments in terms of clinical challenges. In case of extensive burn injuries, these grafts have failed to cover a large body surface area due to the unavailability of donor sites [11]. Typically, alternative skin substitutes are adopted to facilitate angiogenesis and healing, but unfortunately, these substitutes cannot replace normal skin functionality and integrity [12].

Growing evidence indicates that stem cell therapy holds great therapeutic potential to reduce these translational gaps in wound treatments [13]. The self-renewal and multipotent differentiation capabilities of MSCs make them the best candidates for the regeneration of damaged tissues. These MSCs can be isolated from various tissue sources, but human umbilical cord-derived MSCs have great potential for wound repair. These cells are capable of migrating in response to a signaling cascade by various paracrine factors and cell-cell interactions [14]. In the therapeutic regimen, MSC transplantation depends on the severity and pathological conditions of the injury [15]. A single local injection of MSCs into the peripheries of the wound is sufficient to exhibit a therapeutic effect [16,17]. However, the survival and integration (homing) of transplanted MSCs are difficult in the harsh wound environment [18,19]. This is a major challenge of MSC-based therapies [20]. Therefore, preconditioning of MSCs with bioactive molecules is an alternative therapeutic approach to overcome this significant concern [17,21]. The survival of transplanted MSCs can be enhanced by exposing them to a hostile microenvironment, due to which cells can adapt to stress (hypoxic) conditions to tolerate severe oxidative and inflammatory wound environment [22].

Medicinal plants contain a variety of bioactive compounds, which make them highly effective in treating skin wounds. Among them, monoterpenes are mainly reported to have relevant pharmacological properties. From this larger class of monoterpenes, alpha terpineol (αT) possesses potent anti-inflammatory, antioxidant, and anti-microbial activity required for efficient wound healing [23]. It is a cytoprotective compound reported to reduce inflammation, oxidative stress, nitric oxide production, and *TNF-α* levels, thereby promoting the healing process [24,25]. Considering these remarkable properties of αT, the current study was designed to evaluate its combined effect with MSCs in enhancing the healing of full thickness acid burn wounds.

## 2. Materials and methods

### 2.1. Chemicals/reagents

Analytical or molecular grade chemicals/reagents were used in this study. These include Alpha terpineol (αT) (SHBL9134, Sigma-Aldrich), Bright green 2X qPCR master mix (G892, Applied Biological Materials Inc.), 4′,6-diamidino-2-phenylindole (DAPI, 157574, MP Biomedicals), 3-[4,5-dimethylthiazol-2-yl]-2,5 diph enyl tetrazolium bromide (MTT, M5655, Sigma-Aldrich), Dimethyl sulfoxide (DMSO, 196055, MP Biomedicals), Fetal Bovine Serum (FBS, 10438-026, Gibco), Hematoxylin & Eosin (H & E), Masson's trichrome (T.864.1, Carl-Roth), Ketamine hydrochloride (K2753-5G, Sigma-Aldrich), α-Minimum essential medium (α-MEM, 12561-056, Gibco), One-step RNA reagent (BS410A, Bio Basic), Paraformaldehyde (PFA, P087.1, Carl Roth), Penicillin/streptomycin (15140-122, Gibco), Phosphate buffered saline (PBS, 70011-044, Gibco), RevertAid First Strand cDNA synthesis kit (K1622, Thermo Scientific), Sodium pyruvate (11360, Gibco), Sulfuric acid (31350, Fluka, Riedel-dehaen), Triton X-100 (T8787, Sigma-Aldrich), Trypsin-EDTA (25200056, Gibco), Trizol (15596026, Thermo Scientific), Tween 20 (194724, MP Biomedicals), Xylazine hydrochloride (A148943-5, Ambeed Hts).

### 2.2. Ethical approval

All experiments were conducted as per the ethical guidelines of respective ethical committees. Tissue samples were collected from Zainab Panjawani Memorial Hospital after the donors' informed consent and cesarean section. The protocol of MSC isolation was approved by the local independent ethical committee, International Center for Chemical and Biological Sciences (IEC, ICCBS), University of Karachi (IEC/ICCBS-036-HT-2018/Protocol/1.0). Animal surgery was performed according to the international guidelines for the care and use of laboratory animals (Animal Study Protocol number ICCBS-ASP-7-2022-008).

### 2.3. Isolation and propagation of MSCs

MSCs were isolated and cultured following the procedure described in our previous studies [17,21]. Briefly, the umbilical cord was washed with 1X PBS to remove blood clots and then cut into small pieces (3–5 mm). The tissue explants were transferred into T-75 flasks containing α-MEM supplemented with 10% FBS and 100 units/mL penicillin and streptomycin. After 10–15 days, cells extended from the explants and adhered to the surface of the flasks. Once the cells reached 90% confluency, adherent cells were detached *via* 1X trypsin-EDTA and subcultured in a fresh medium to the next passage. The exhausted medium was replaced every third day, and cells were observed under a phase contrast microscope (TE2000 Nikon, Japan).

### 2.4. Characterization of MSCs

Isolated MSCs were maintained for subsequent passages, and their identification was confirmed by morphological characteristics, potential to differentiate into multiple (osteogenic, chondrogenic, and adipogenic) lineages, and expression of MSC-specific markers *via* immunoctochemistry and flow cytometry.

#### 2.4.1. Multipotent differentiation

MSCs were cultured in a 6-well plate with 75% confluency and incubated with a specific induction medium to induce differentiation into trilineage. Medium for osteogenic differentiation comprised 10 μM Insulin, 1 μM Dexamethasone, and 200 μM Indomethacin. The chondrogenic induction medium contained 10 ng Insulin, 1 μM Dexamethasone, 20 ng TGFβ1, and 100 μM Ascorbic acid. The adipogenic induction medium consisted of 1 μM Dexamethasone, 10 μM Insulin, and 200 μM Indomethacin. Cells were incubated in these respective media which were replaced every 72 h. After 21 days, cells were fixed with 4% PFA for 15 min at room temperature (RT). Following fixation, the differentiated cells were

identified by using specific stains, including 1% Alcian (chondrocytes), 25% Alizarin red (osteocytes), and Oil Red O (adipocytes). Stained cells were detected under a bright field microscope (NIE, Nikon, Japan).

#### 2.4.2. Immunocytochemistry

The protocol for immunocytochemistry was described previously [26]. In brief, cultured cells were fixed with 4% PFA for 20 min and permeabilized with 0.1% Triton X-100. Cells were incubated in a 2% blocking solution for 30 min. MSC-specific markers (CD29, CD90, Stro-1, Vimentin) were used with monoclonal primary antibodies. Hematopoietic marker CD45 (MSC negative marker) was also used for confirmation. These cells were incubated in the dark with Alexa fluor 546 goat anti-mouse secondary antibody, and phalloidin (1:200) for 1 h for cytoskeleton (actin filaments) staining. Nuclei were stained with 0.5 μg/mL DAPI. Immunofluorescence of stained cells was observed under a fluorescence microscope (NIE, Nikon, Japan).

#### 2.4.3. Flow cytometry

Cells were further characterized and quantified by flow cytometric analysis. Confluent MSCs were washed with PBS and detached using a cell dissociation solution. Primary antibodies (CD105, CD73, CD90 and CD44) with recommended dilutions were added to the cell suspension and incubated at 37 °C for 1 h. FACS solution (1 mM EDTA, 1% BSA, 0.1% sodium azide in PBS) was used for washing. Cells were labeled with Alexa fluor 546 goat anti-mouse secondary antibody (1:200) and examined *via* a flow cytometer (FACS Celesta, Becton Dickinson).

### 2.5. Cytotoxicity of alpha terpineol (αT)

Before preconditioning, the cytotoxicity of αT was determined *via* trypan blue and MTT colorimetric assays. The protocol was performed as described in our previous studies [26,27]. MTT assay was performed to evaluate the metabolic activity of MSCs after αT exposure. Briefly, approximately 7000 cells were allowed to grow in 96-well plate at 37 °C. Once the cells formed a monolayer, different concentrations (5–50 μM) of αT were added to the appropriate wells, along with serum free media for 24 h. The media were removed after 24 h and MTT solution (5 mg/mL) was added for 4 h. To dissolve the crystals formed by MTT, 200 μL DMSO (dimethyl sulfoxide) was added to each well for 2 min followed by measuring absorbance at 570 nm *via* a spectrophotometer (Multiskan FC microplate photometer, Thermo Scientific, US). Trypan blue assay was further performed to confirm the cell viability after αT exposure. Cells ($1 \times 10^4$/mL) were grown with confluent monolayer in a 6-well plate and exposed to the same concentrations of αT for 24 h. Next, treatment was removed, cells were trypsinized, and resuspended in 1 mL of fresh PBS. Cells were counted by mixing equal volumes (10 μL) of the cell suspension and 1X trypan blue. The combined suspension was loaded in a hemocytometer and the number of viable and non-viable cells were counted under a phase contrast microscope.

### 2.6. Preconditioning of MSCs

After the identification of a non-cytotoxic concentration of αT, MSCs were preconditioned with this optimized concentration for 24 h. Next day, the morphological characteristics of the preconditioned cells were examined under a phase contrast microscope. Treatment was removed, and cells were trypsinized and used for subsequent experiments.

### 2.7. Cell migration via scratch assay

Scratch assay was performed to examine the relative migration of MSCs after preconditioning with αT. A scratch was induced in the cell monolayer of normal or αT-MSCs, followed by washing with 1 X PBS. The culture was maintained with serum-free medium till 72 h. Cell migration was observed from the time of the scratch induction ($t = 0$ h) till the complete healing/filling of the scratch ($t = 72$ h), and quantified using ImageJ software.

### 2.8. Experimental animals

Animals (rats) were housed in the institutional animal resource facility and maintained at 24 ± 2 °C with a relative humidity of 55% ± 5% and 12 h light/dark cycle, with access to food and water *ad libitum*. Animals comprised ($n = 46$) male Wistar rats (180–220 g) for developing full thickness acid burn wounds. Initially, $n = 10$ rats were used to optimize the full thickness acid burn wound model. Rats were randomly divided into three main groups: control (burn model), group 1 (wound + normal MSCs), and group 2 (wound + αT-MSCs). Each group was divided into two sub-groups based on the early (day 10) and late (day 40) phases of wound healing, with the number of animals ($n = 6$) in each sub-group.

### 2.9. Acid burn wound model

A combination of ketamine hydrochloride (60 mg/kg) and xylazine hydrochloride (7 mg/kg) was injected intraperitoneally into rats to induce anesthesia. Hair from the dorsal surface was removed, and 50 μL of sulfuric acid (97% concentrated) was carefully spread to an area of 3 cm on the skin using a glass dropper. The skin was exposed to the acid for 1 min and then rinsed with deionized water. A combined dose of antibiotics (penicillin and streptomycin 10,000 U/mL) was subcutaneously injected into the rats to avoid the chances of infection. The rats were placed back in their cages with full access to water and food. Digital images were captured to monitor wound healing patterns from the day of wound induction till day 40.

### 2.10. Cell labeling and transplantation

DiI dye, a labeling dye, was used to track transplanted cells. MSCs were trypsinized, and the cell pellet was washed twice with 1X PBS. The pellet was resuspended in 1 mL dye solution (5 μM dissolved in serum free-medium) and incubated for 7 min. Next, the serum-containing medium was added and centrifuged at 1000 rpm for 8 min to stop the reaction. The pellet was again washed twice and resuspended in 300 μL of 1 X PBS. Same labeling method was followed for the αT-MSCs. Both normal and αT-MSCs were carefully transplanted into the animal model after 48 h of burn wound induction. Only a single dose of cells ($2 \times 10^6$ cells) was subcutaneously injected at multiple peripheries of the wound. After transplantation, labeled cells were quantified through their fluorescence intensities by using ImageJ software.

### 2.11. Macroscopic analysis

After wound induction, general manifestation (wound lesions, body weight) was observed. Macroscopic changes (edema, erythema, infections, blistering, crust, tissue granulation, and re-epithelization) were also noted with or without treatments. To monitor the progression of wound healing, digital images were captured at regular intervals (3–5 days) till the end of the experiment (day 40).

### 2.12. Tissue harvesting and evaluation

Animals were euthanized, and their respective wound tissues were harvested from the center of the lesions. Tissues were collected in the early (day 10) and late (day 40) phases of wound healing and evaluated *via* histological, immunohistochemical, and gene expression analyses.

#### 2.12.1. Histological examination

Histological examination and scoring were performed to evaluate the structural integrity, inflammation, collagen content, and epidermal regeneration after wound induction. Harvested tissues were processed for Hematoxylin & Eosin (H & E), and Masson's trichrome staining as per the manufacturer's instructions.

*2.12.1.1. Tissue processing and staining.* Tissues were immediately fixed with 4% PFA overnight and subsequently dehydrated in a gradually reduced concentration of isopropyl alcohol. Dehydrated tissues were embedded in paraffin and sectioned into 6 μm thick sections. Subsequently, sections were deparaffinized and rehydrated to restore their water content or structural integrity. The sections were stained with Hematoxylin for 1 min and washed with distilled water. One drop of eosin was added for 30 s to differentiate nuclei and cytoplasmic content. Tissue collagen was examined by Masson's trichrome staining. Initially, Wiegert's iron hematoxylin was added to the tissue sections, followed by the addition of aniline blue dye to impart a distinct color. One drop of phosphomolybdic acid was added to differentiate the tissue content. Lichun red acidic magenta was poured to enhance the staining by removing extra stains and washed with glacial acetic acid. Histological images were visualized under bright field microscope.

*2.12.1.2. Tissue scoring.* All tissues after staining were scored based on tissue necrosis, collagen deposition, tissue granulation (neoformed connective tissue), and skin adnexa. For instance, tissue scoring (0–3; 0 = normal, 1 = mild, 2 = medium, and 3 = extensive) was performed at corresponding time points (days 10, 40) and verified by blind review of a pathologist. A final average score was given to each section after critical evaluation.

#### 2.12.2. Immunohistochemical examination

Tissues were analyzed to detect blood vessel density and leukocyte infiltration at day 40. Primary antibodies, including α-smooth muscle actin (α-SMA) and CD18, were used to stain blood vessels and infiltrating leukocytes, respectively. Parafinized embedded sections were deparaffinized and rehydrated with gradually increased concentrations of isopropyl alcohol. These sections were processed for antigen retrieval in sodium citrate buffer at 95 °C for 10 min, followed by washing with PBS-tween 20 buffer. Sections were treated with a 2% blocking solution for 30 min to prevent non specific binding. Respective monoclonal primary antibodies (1:100) were added to the sections and incubated at 4 °C overnight. Alexa fluor secondary antibodies (488 anti-rabbit; for α-SMA), (546 anti-mouse; for CD18) with 1:200 dilutions were added for 2 h at 37 °C and washed thrice with PBS-tween 20 buffer. Nuclei were stained using DAPI (1: 1000), and sections were mounted with a DPX mounting medium. The stained sections were examined under a fluorescence microscope.

#### 2.12.3. Gene expression profile of wound healing mediators

*2.12.3.1. RNA extraction.* Total RNA was extracted from tissues (100 mg) *via* Trizol reagent, following manufacturer's guidelines. The same protocol was followed as mentioned in our previous study [27]. Briefly, tissues were homogenized, crushed in liquid nitrogen, and transferred into 1 mL Trizol reagent. β-mercaptoethanol (3.5 μL) was added and incubated at 70 °C for 20 min. Next, 500 μL chilled chloroform was mixed, followed by 15 min incubation. The mixture was centrifuged at 12000×*g* for 15 min to obtain three different layers. Pure RNA from the top layer was transferred to a new tube, and subsequently, 500 μL of 100% isopropanol was added, followed by incubation at 2000×*g* for 10 min. The resultant RNA pellet was washed twice with 100% ethanol and reconstituted into nuclease-free water. RNA was quantified *via* spectrophotometer (NanoDrop 2000, Thermo Scientific, USA) and absorbance was measured at 260 nm.

*2.12.3.2. cDNA synthesis.* Extracted RNA (1 μg) was used for cDNA synthesis using the RevertAid First Strand cDNA synthesis kit under the given recommendations of the manufacturer. In a microcentrifuge tube, 10 μL of nuclease-free water, 1 μL of the random hexamer, 1 μL of RNA sample, 4 μL of 5 X reaction buffer, 1 μL of RiboLock RNase Inhibitor, 2 μL of dNTPs, and 1 μL of RevertAid Reverse transcriptase, were added. The tube was centrifuged for a short spin and kept in the thermal cycler for the following incubation cycles: 25 °C for 10 min, 42 °C for 60 min, and 70 °C for 10 min. The synthesized cDNA was stored at −20 °C.

*2.12.3.3. Quantitative real-time PCR (qPCR).* Synthesized cDNA was mixed with the 1:10 dilution of Bright green 2X qPCR Master Mix. A PCR plate was prepared by adding 5 μL of primer solution (1: 100) and 5 μL of cDNA mixture. Primer details are given in Table 1. Each sample analysis was performed in triplicate, and the amplification of each gene was normalized with the corresponding housekeeping gene (GAPDH). Next, the prepared PCR plate was run in the qPCR machine (CXF96 Touch Real-Time PCR Detection System, Bio-Rad, USA) and the fold change, 2 - (ΔΔCt) of each gene was calculated.

### 2.13. Data analysis

Data was represented as mean ± SEM and analyzed by GraphPad Prism (8.0.2). Image J and Adobe Photoshop software were used for data visualization and quantification. Statistical tests, including unpaired *t*-test and One-way ANOVA followed by Tukey post hoc analysis, were performed to measure differences between two or

**Table 1**
Targeted genes with their specific primer sequences.

| Genes | Primer Sequence (5'-3') (Forward) | Primer Sequence (5' -3') (Reverse) |
|---|---|---|
| *GAPDH* | GGAAAGCTGTGGCGTGATGG | GTAGGCCATGAGGTCCACCA |
| *IL-1β* | TCATCTTTGAAGAAGAGCCCGT | GTTCTGTCCATTGAGGTGGAGA |
| *IL-6* | GATGGATGCTTCCAAACTGGATA | TGAATGACTCTGGCTTTGTCTTT |
| *TNF-α* | CCTCTTCTCATTCCTGCTCGT | GATCTGAGTGTGAGGGTCGG |
| *IL-13* | TGGCTCTCGCTTGCCTT | GCCAGCTGTCAGGTCCA |
| *Bax* | GATCTGAGTGAGGGTCTGG | CTTCTTCCGTGTGGCAGC |
| *BCL-2* | TTCCCGTGCAATCAGTTCGG | TCCAGGTGTCGTTGCGG |
| *PRDX-4* | CAAAGCCACGGCTGTTATGC | TGGGTCCCAATCCTCCTTGT |
| *GPX-7* | AGGAGATCAAGCCCCGTAT | CGAAGGGAAGAGAAGCATT |
| *SOD-1* | GTGGCCAATGTGTCCATTGAAG | CAATCCCAATCACACCACAAGC |
| *TGF- β* | CACTGCTCTTGTGACAGCAAA | CGGTTCATGTCATGGATGGTG |
| *PDGF* | TTCACCAGAGCGGAC | TGTGGAGGTGGAAGCGAG |
| *VEGF* | CCAATTGAGACCCTGGTGGA | TCCTATGTGCTGGCTTTGGT |
| *FGF* | AGCAGAAGAGAGAGGAGTTGTG | TATTTCCGTGACCGGTAAGTGT |
| *EGF* | TAACGGGCCTGACAGCA | TGCACTGGCCCGAGTTA |
| *MMP-9* | TACCAGCTACTCGAACCAATCA | AAATAAAAGGGCCGGTAAGGTG |

GAPDH: Glyceraldehydes-3-phosphate dehydrogenase, IL-1β: Interleukin-1 beta, IL-6: Interleukin 6, TNF-α: Tumor necrosis factor alpha, IL-13: Interleukin 13, Bax: Bcl-2-associated X protein, BCL-2: B-cell leukemia/lymphoma 2 protein, PRDX-4: Peroxiredoxin 7, GPX-7: Glutathione peroxidase-7, SOD-1: Superoxide dismutase-1, TGF-β: Transforming growth factor-beta, PDGF: Pletelete derive growth factor, VEGF: Vascular endothelial growth factor, FGF: Fibroblast growth factor, EGF: Epidermal growth factor, MMP-9: Matrix metalloproteinase-9.

multiple groups, respectively. A threshold of $p \leq 0.05$ was considered statistically significant ($*p \leq 0.05$, $**p \leq 0.01$, $***p \leq 0.001$).

## 3. Results

### 3.1. Identification of MSCs

Growth of MSCs was extended from the explant after the 10th day of culturing, designated as passage 0 (P0) cells. Subsequently, MSCs exhibited a consistent spindle-shaped, fibroblast-like morphology in all sub-cultured passages (P1 and P2) (Fig. 1A). In addition, MSCs were successfully differentiated into chondrocytes, adipocytes, and osteocytes after specific staining. Oil Red O stained oil droplets of adipocytes, Alcian blue stained ECM content of chondrocytes, and Alizarin red stained minerals deposits of osteocytes (Fig. 1B). Immunocytochemical analysis demonstrated that MSCs were positive for CD29, CD90, Stro-1, Vimentin, and negative for CD45 (Fig. 1C). Similarly, the expression levels of CD105, CD73, CD90, and CD44 were analyzed *via* flow cytometry, as illustrated in Fig. 1D.

### 3.2. Cytotoxic evaluation

According to the cytotoxicity analysis, 10 μM concentration of αT was identified as the safe concentration for preconditioning for cell migration analysis as well as *in vivo* transplantation (Fig. 2A). The αT-MSCs showed same morphological appearance as observed in case of normal cultured MSCs (Fig. 2B). However, αT showed a positive effect on the growth of MSCs as evidenced by the enhanced proliferation and migration.

### 3.3. Alpha terpineol preconditioning enhanced cell migration

The migration capability of MSCs was analyzed by scratch assay in the absence and presence of αT treatment. αT-MSCs exhibited enhanced cell migration (blue arrows) and complete wound closure (scratch area) in contrast to the control (normal MSCs) (Fig. 3A). Wound closure was quantified at respective time points; scratch was completely filled by significantly enhanced ($p \leq 0.05$) migration of αT-MSCs with relative percentages; 45% (24 h), 71% (48 h), and 92% (72 h). Conversely, normal MSCs showed incomplete wound closure with relative percentages of 20% (24 h), 51% (48 h), and 68% (72 h) (Fig. 3B).

### 3.4. Characterization of full thickness acid burn wound

Full thickness acid burn wound was characterized based on the macroscopic and microscopic examinations. Gross macroscopic observation revealed that all skin layers (epidermis, dermis, and hypodermis) were damaged after acid exposure (Fig. 4A). The physical appearance of the wound (white, dry feather-like crusty hard lesion) was noted with a foul smell. Microscopic examination *via* histology exhibited devastated collagen fibers along with skin appendages and layers (Fig. 4B). It was further confirmed by the gene expression analysis, which showed substantial ($p \leq 0.05$) upregulation of inflammatory (*IL-1β*, *IL-6*, *TNF-α*), oxidative stress (*SOD-1*, *PRDX-4*, *GPX-7*), and apoptotic markers (*Bax and BCL-2)* in the burn wound tissue (Fig. 4C). All these observations were critically analyzed by comparison with normal rat skin confirming that the full thickness burn wound model was successfully developed.

### 3.5. MSCs enhanced full thickness acid burn wound healing

To examine the potential of MSCs in full thickness burn wound healing, approximately $2 \times 10^6$ cells (normal MSCs and αT-MSCs) were subcutaneously injected after 48 h of burn wound induction. The control group (burn model) was monitored without any treatment. Group 1 received normal MSCs, while group 2 received αT-MSCs, in a single dose at three different wound peripheries.

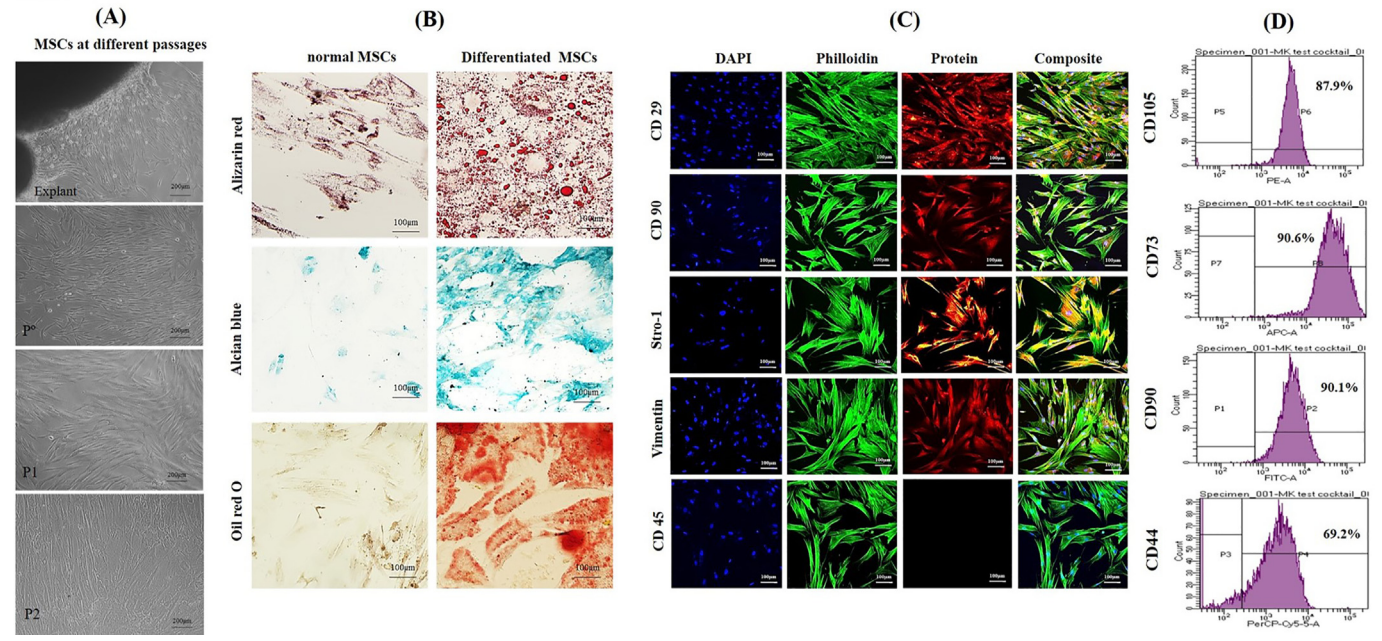


**Fig. 1.** MSC characterization. **(A)** Phase contrast microscopic images showed a homogenous population of MSCs from umbilical cord tissue explant. MSCs were identified based on the adherent capability and spindle-shaped fibroblast-like morphology, scale bar = 200 μm, **(B)** Potential of MSC differentiation into adipocytes (Alizarin red), chondrocytes (Alcian blue), and osteocytes (Oil red O), scale bar = 100 μm, **(C)** Confirmation of MSCs in culture by the relative expression of specific markers by immunocytochemistry. MSCs were positive for CD29, CD90, Stro-1, and Vimentin and negative for CD45 observed under fluorescent microscope, scale bar = 100 μm. **(D)** Flow cytometry revealed positive expression of CD105 (87.9%), CD73 (90.6%), CD90 (90.1%), and CD44 (69.2%).

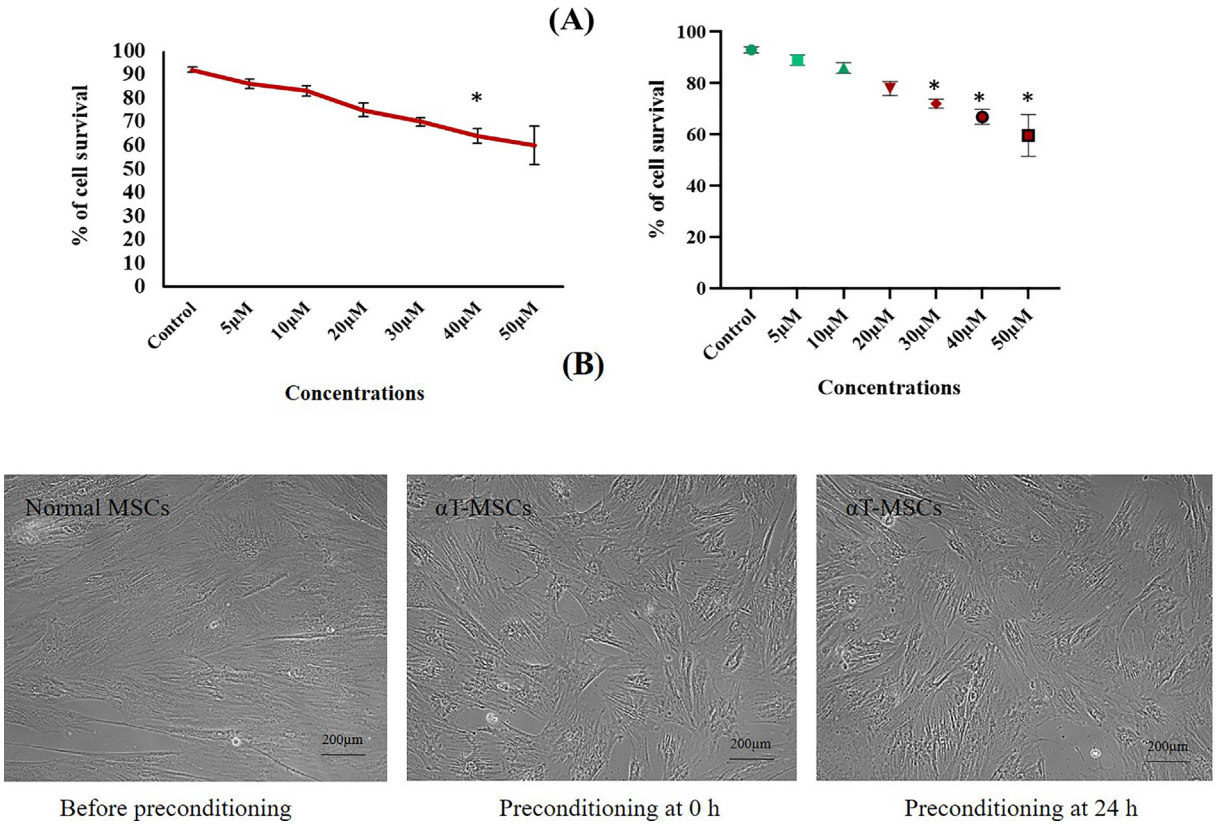


**Fig. 2.** Alpha-terpineol cytotoxicity analysis and preconditioning of MSCs. **(A)** Cell viability and metabolic activity were determined by trypan blue and photometric MTT assays, respectively. Both assays identified 10 μM as a non-cytotoxic concentration of the compound. **(B)** Phase contrast microscopic images show the phenotypic characteristics of MSCs before and after preconditioning. No significant changes were observed in the morphology of MSCs, scale bar = 200 μm.

During the early phase, an increased number of labeled (homed) cells were observed in group 2 as compared to group 1 (Fig. 5A). Healing pattern (crusty scab formation, scab detachment, bleeding, and wound contraction) was examined till day 40. Findings revealed extensive damage and necrosis with incomplete wound healing in the control group. Control group showed skin wound repair by forming multiple scabs, but due to the aggressive nature of the injury, healing was not observed. Interestingly, both normal and αT-MSC treated groups exhibited a single scab formation followed by detachment, resulting in a remarkable ($p \leq 0.05$) wound contraction at day 40 (Fig. 5B and C).

### 3.6. Histological scoring and quantification

Wound tissues were examined by histological analysis and compared with the normal rat skin *via* a scoring system. Normal rat skin showed intact layers with organized tissue integrity and extracellular matrix (ECM) (Score 0). On day 10, the control group showed destructive integrity of tissue architecture (Score 3). Wound tissue was completely necrotic (≥95%), and all layers were damaged with a devastated collagen network. Among the treated groups, group 1 exhibited deep necrosis (≥67%) with damaged dermal layer and collagen fibers (Score 2). However, mild tissue granulation (≥35%) was also noted. In the case of group 2, same parameters were examined with less necrosis (≥46%) and significant tissue granulation with partial collagen deposition (≥50%). These parameters indicated that group 2 followed a normal cascade of wound healing after αT-MSC treatment (Fig. 6A). All tissues were further evaluated and scored at day 40. At this phase, dermal regeneration necessitates the fine deposition of the collagen fibers, which is facilitated by the fibroblasts and myofibroblasts. As shown in Fig. 6B, Masson's trichrome staining revealed damaged collagen with poor reconstruction of skin adnexa in the control group (Score 2). After treatments, group 2 (Score 0) exhibited well-reorganized collagen fibers (≥98%), tissue granulation (≥95%), and regenerated skin adnexa (≥82%) as compared to group 1 (Score 1). This result was consistent with the macroscopic observation where significant wound closure was noted in group 2 as compared to the other groups.

### 3.7. αT-MSCs reduced leukocyte infiltration and enhanced neovascularization

Histological examination was further supported by immunofluorescence staining of the infiltrated leukocytes at day 40. A crucial adhesion molecule called CD18 or CD11d is involved in the recruitment of leukocytes. In the control group, CD18 was highly expressed, which may significantly influence the intricate cascade of wound healing. However, group 1 also exhibited a slightly positive expression of CD18 along with wound contraction. This observation may suggest that the inflammatory response was not effectively suppressed, and the wound failed to heal completely. Interestingly, accumulation of leucocytes was not observed in group 2, indicating that αT-MSCs play a significant role in inhibiting CD18 function and reducing leukocyte infiltration, thus improving the wound healing process (Fig. 7A).

At the same phase of wound healing, α-SMA expression was examined in all experimental groups, including normal skin. It is a specific fibrogenic and endothelial marker that is widely used to assess injury-associated angiogenesis and fibrogenesis. α-SMA was markedly expressed in normal skin (Fig. 7B). However, the density of matured vessels at the wound center was considerably higher

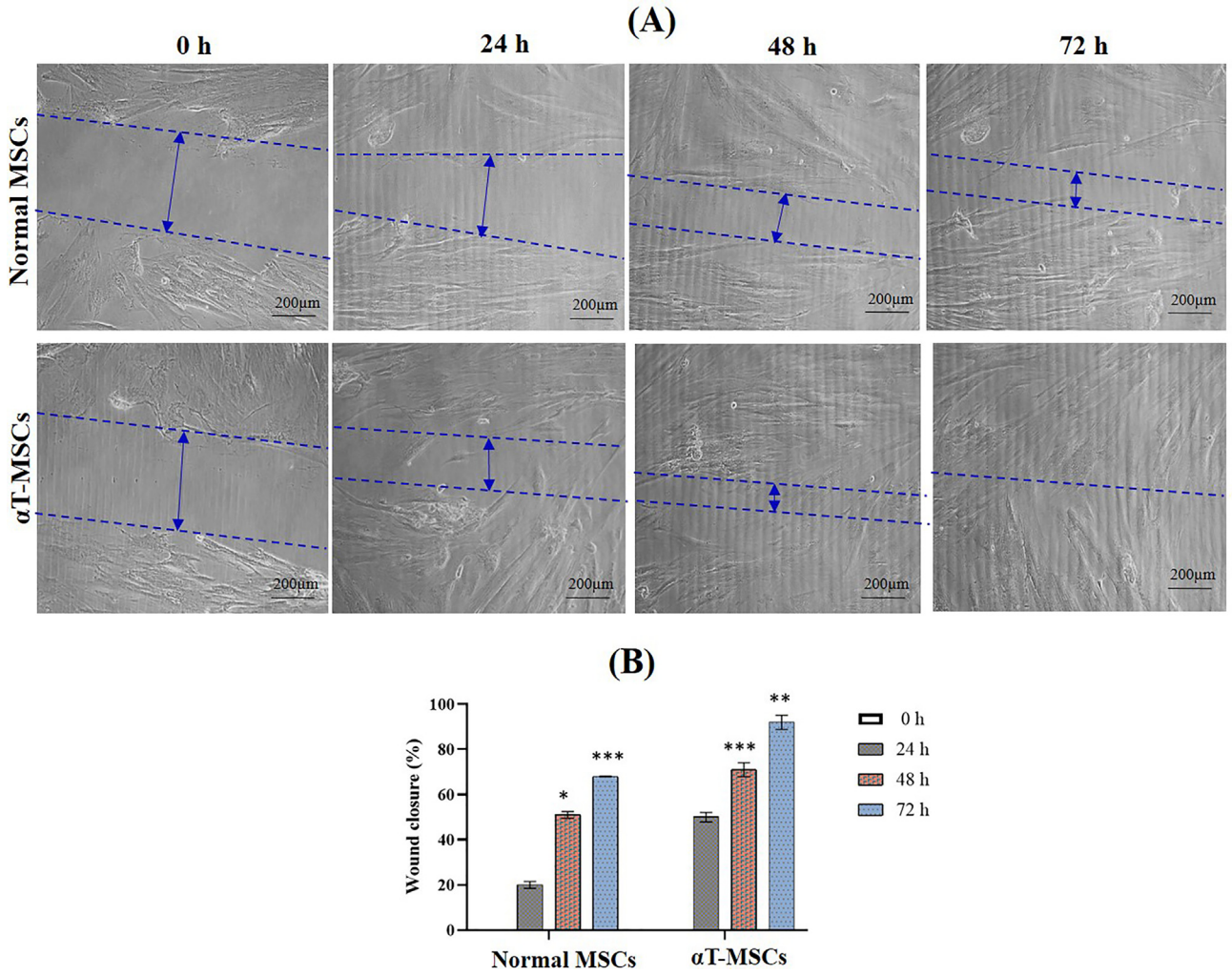


**Fig. 3.** Alpha-terpineol (α-AT) preconditioning enhanced cell migration. **(A)** Phase contrast microscopic images show MSC migration at 0, 24, 48, and 72 h *via* scratch assay analysis. Blue arrows indicate the area of wound closure (scratch) in the normal and αT-MSC groups, scale bar = 200 μm. **(B)** Bar graphs display statistical quantification of wound closure (%) at 0, 24, 48, and 72 h in both groups. One-way ANOVA with the Bonferroni post-hoc test was performed *via* IBM SPSS Statistic 21 software, and *p*-values ≤0.05 were considered statistically significant (*** = $p \leq 0.001$, ** = $p \leq 0.01$, and * = $p \leq 0.05$).

($p \leq 0.05$) in both groups 1 and 2 than in the control group (Fig. 7C). These results demonstrate that MSCs can rapidly and efficiently promote blood vessel formation, thereby enhancing neovascularization.

### 3.8. Gene expression profile of wound healing factors

Temporal changes in the gene expression of the wound tissues were evaluated at days 10 and 40 (Fig. 8A and B). In comparative analysis with the normal skin, control group exhibited significantly higher levels of inflammatory (*TNF-α, IL-6, and IL-1β*) and apoptotic (*Bax*) cytokines. It indicates that normal skin did not exhibit any aberrant physiological response (inflammation, apoptosis). Similarly, the gene expression profile of angiogenic (*VEGF, FGF*) and remodeling (*EGF, PDGF, TGF-β, MMP-9*) markers were substantially downregulated in the control group, representing poor angiogenesis and skin repair mechanism. Further, a significant reduction in the *TNF-α, IL-6, IL-1β,* and *Bax* levels was observed in group 2 in contrast to other groups. Conversely, the anti-oxidative gene profile of the normal and αT-MSC treated groups at day 10 showed increased levels of *PRDX-4, GPX-7, and SOD-1* compared to the control group. Moreover, the gene expression profiles of angiogenic and remodeling cytokines were also elevated in group 2 compared to group 1. Transplanted αT-MSC showed an effective therapeutic response against inflammation and oxidative stress and accelerated significant wound closure.

## 4. Discussion

Skin wounds, including full thickness burns, pressure sores, and diabetic foot ulcers, have a detrimental impact on patient's health and socio-economic stability. These wounds are characterized by a prolonged inflammatory phase and excessive secretion of reactive oxygen species (ROS), either locally or invasively, necessitating urgent effective interventions [28]. The available therapeutic approaches comprise only surgical debridement and autologous skin grafting, but due to the large area of burned skin, patients' skin is unable to cover the damaged area [29]. Recently, the exogenous (local) application of MSCs has gained significant attention as a promising area of investigation in preclinical studies [30]. The primary focus of this therapeutic approach is to enhance the overall efficacy and outcome of the wound healing process. Many investigations have demonstrated that human umbilical cord-derived MSCs (hUCMSCs) can secrete various cytokines and growth factors that facilitate skin wound regeneration [31]. However, a hypoxic wound microenvironment comprises elevated

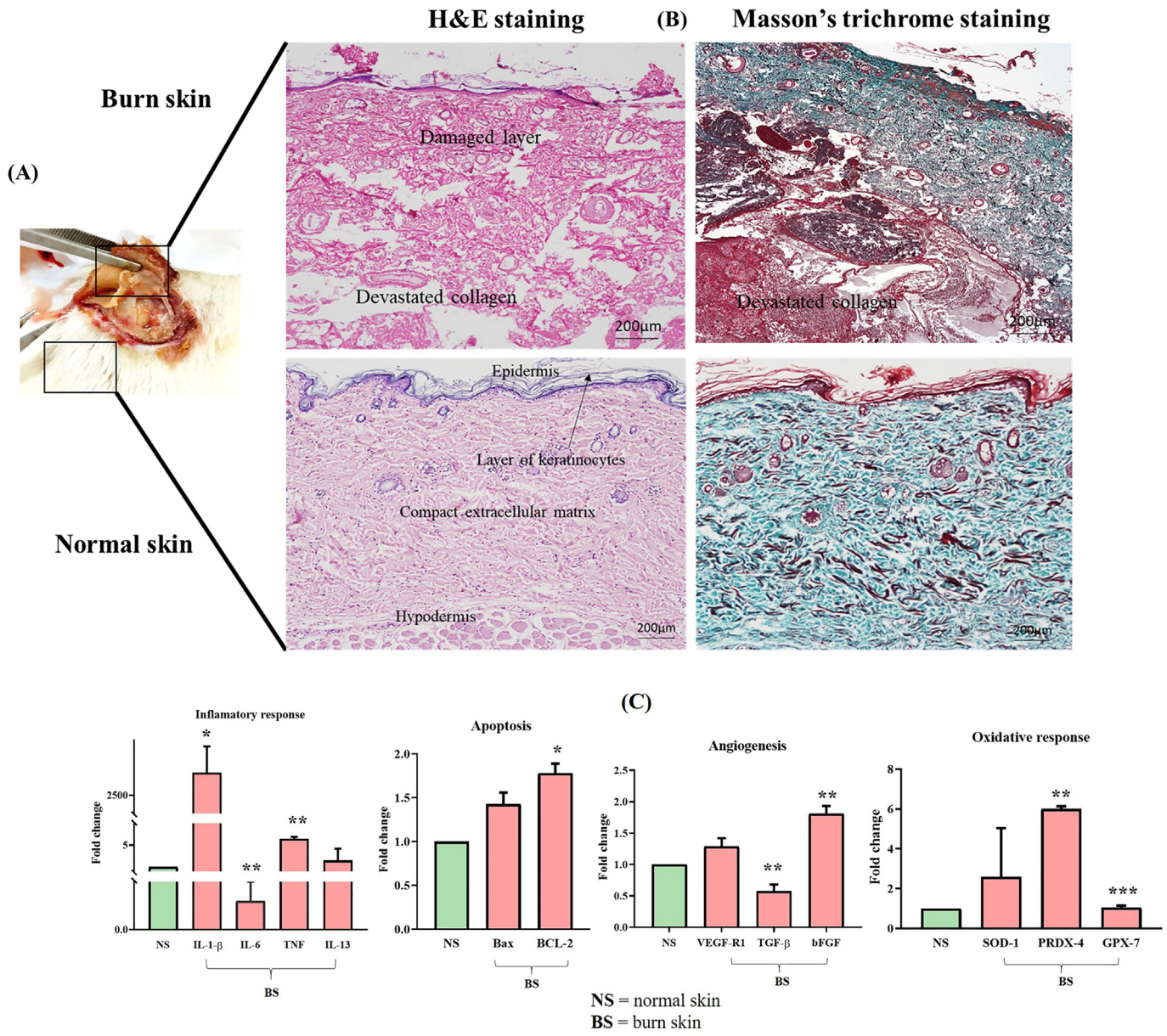


**Fig. 4.** Characterization of full thickness acid burn wound. **(A)** Gross macroscopic appearance of the destructive tissue shows that all layers were damaged after acid burn wound induction. **(B)** Histological evidence of the damaged tissue *via* staining with H & E and Masson's trichrome. **(C)** Wound was also confirmed by significantly increased expression of wound healing factors *via* qPCR analysis in the burn skin tissue as compared to the normal skin tissue. Student's t independent test was performed using IBM SPSS Statistic 21 software, and *p*-values ≤0.05 were considered statistically significant (*** = $p \leq 0.001$, ** = $p \leq 0.01$, and * = $p \leq 0.05$).

levels of inflammatory factors and ROS that pose significant challenges to the viability and homing of the MSCs [28]. This limitation can be effectively overcome by using cytoprotective compounds exhibiting anti-oxidative, anti-inflammatory, and wound healing properties [13]. Many plant extracts and phytochemical compounds (flavonoids, terpenoids, phenols, etc.) have been employed and regarded as traditional remedies for managing different types of burn wounds [32]. These compounds can precondition MSCs, thereby enhancing their homing and overall survival following transplantation.

In this study, we selected α-Terpineol (αT), which belongs to the family of monoterpenes and is commonly found in essential oils. It is known for having cytoprotective effects and biological activities against wound healing by inhibiting interleukins (ILs) and ROS production [23]. Despite their significant relevance, the wound healing potential of αT has not been extensively examined. Here, we explored the synergistic effect of αT and MSCs *via* a preconditioning approach in both *in vitro* and *in vivo* experiments. In cell functional scratch assay, enhanced wound closure (scratch gap) was observed in the αT-MSC group compared to the normal MSC group. MSCs, after preconditioning, not only exhibited enhanced migration but also showed substantial cell proliferation, confirming the cytoprotective effect of αT. Similar therapeutic effect of αT-MSCs was also noted in the animal study. This is the first study documenting a preclinical model of full thickness acid burn wounds induced by sulfuric acid. Direct contact with concentrated acid results in significant damage to all layers of the skin. This wound was effectively characterized through visual macroscopic and histological observations with and without treatment. Macroscopic observation of the affected skin exhibited evident signs of tissue

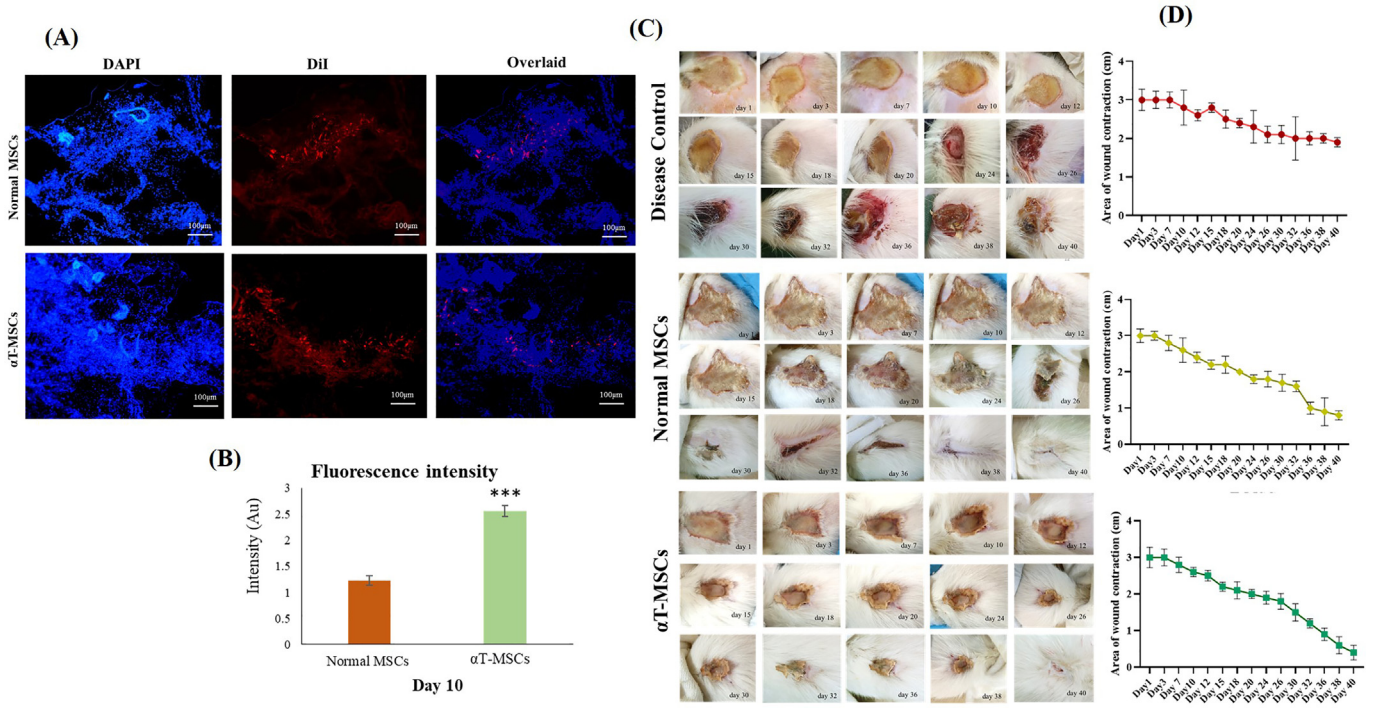


**Fig. 5.** Macroscopic examination of acid burn wounds and cell tracking. **(A)** Fluorescent microscopic images show homing of the labeled MSCs (red) during the early phase of wound healing (day 10). DAPI was used to visualize cell nuclei, scale bar = 100 μm (20X). **(B)** Bar graph shows fluorescence intensity of labeled MSCs in group 1 compared to group 2. **(C)** Digital photographs exhibit wound healing patterns (crusty scab formation, scab detachment, bleeding, and wound contraction) at regular intervals (3–5 days) till day 40. **(D)** Graphical representation exhibits area of wound contraction in all experimental groups. One-way ANOVA with the Bonferroni post-hoc test was performed *via* IBM SPSS Statistic 21 software, and *p*-values ≤0.05 were considered statistically significant (*** = $p \leq 0.001$, ** = $p \leq 0.01$, and * = $p \leq 0.05$).

damage, characterized by necrosis and foul smell. Wound exhibited extensive necrosis, inflammatory, and oxidative response evaluated by gene expression analysis and histological scoring. Once the wound was established, a single dose of cells (normal and αT-MSCs) was injected after 48 h. Cells were labeled before transplantation and tracked till day 10. Findings show that transplanted αT-MSCs displayed a preferential migration towards the wound bed and homed well as compared to the normal MSCs.

Moreover, αT-MSCs exert their therapeutic effect by modulating the local microenvironment of the wound site. Healing pattern was analyzed till day 40 and exhibited significant wound contraction in the wound treated with αT-MSCs as compared to other groups. Microscopic images confirmed tissue devastation *via* a scoring system. Histological scoring is a pragmatic approach to assess the wound healing progression by evaluating the structural integrity of the damaged tissue [33]. This scoring was distinguished by its intrinsic quantifiability, thereby enhancing the precision and reproducibility of the histological outcomes [34]. In the present study, remarkable changes in the histological parameters were observed and scored based on the healing pattern. Necrosis, dysregulated skin adnexa, tissue granulation, and collagen depositions were the main characteristics noted in the early and late healing phases (Tables 2 and 3). The findings revealed that αT-MSCs exerted a promising effect on tissue architecture, as evidenced by a reduction in necrosis, and enhanced formation of hair follicles (≥82%), tissue granulation (≥95%), and collagen deposition (≥98%). The promising results of epidermal and dermal regeneration were achieved within 40 days after αT-MSC treatment, suggesting that tissue reconstruction occurred without significant necrosis (Supplementary Fig. 1 A and Supplementary Fig. 1 B). These effects were compared and scored between the control and normal MSC treated groups. Same results are in line with the previous findings, in which αT was employed in a biological dressing for wound healing [35]. The transplantation of αT-MSCs was found to induce re-epithelialization and initiate fibroblast activation, thus expediting collagen proliferation. Overall, the quantitative analysis indicated that αT-MSC treatment induces a normal healing cascade in the tissue.

The elucidation of the underlying mechanisms through which αT-MSCs enhanced the wound healing process was done by examining the expression of CD18 and α-SMA. First, leukocyte infiltration was not seen in the αT-MSC group at day 40, as indicated by the absence of CD18 expression. This finding implies a possible inhibition of the inflammatory cascade after αT-MSC treatment. Conversely, the expression of CD18 was found to be significantly upregulated in both the control and normal MSC treated groups. Leukocytes play a crucial role in the innate immune response during wound healing, specifically in transitioning the wound phases from the inflammatory to the proliferative stage. However, their efficacy is limited to 3–5 days post-injury. Therefore, the persistence of infiltration in the wound serves as an indicative marker for aberrant wound regeneration [36]. Secondly, αT-MSCs have been shown to increase the expression of α-SMA significantly, resulting in enhanced neovascularization. It was reported in the previous study that enhanced wound healing was promoted by neovascularization [37]. Thus, this study validated the presence of a sufficient vascular network that promotes the progression of injured tissue toward remodeling, primarily *via* improved neovascularization.

The inflammatory and oxidative responses are the major events of wound healing. The regenerative process might be hindered due to prolonged inflammation as it leads to hypertrophic scarring and fibrosis [38]. In our study, inflammatory genes (*IL-1β, IL-6, TNF-α*) were downregulated and anti-oxidative genes (*PRDX-4, GPX-7, and SOD-1*) were upregulated in the normal and αT-MSCs treated groups as compared to the control group. This finding further

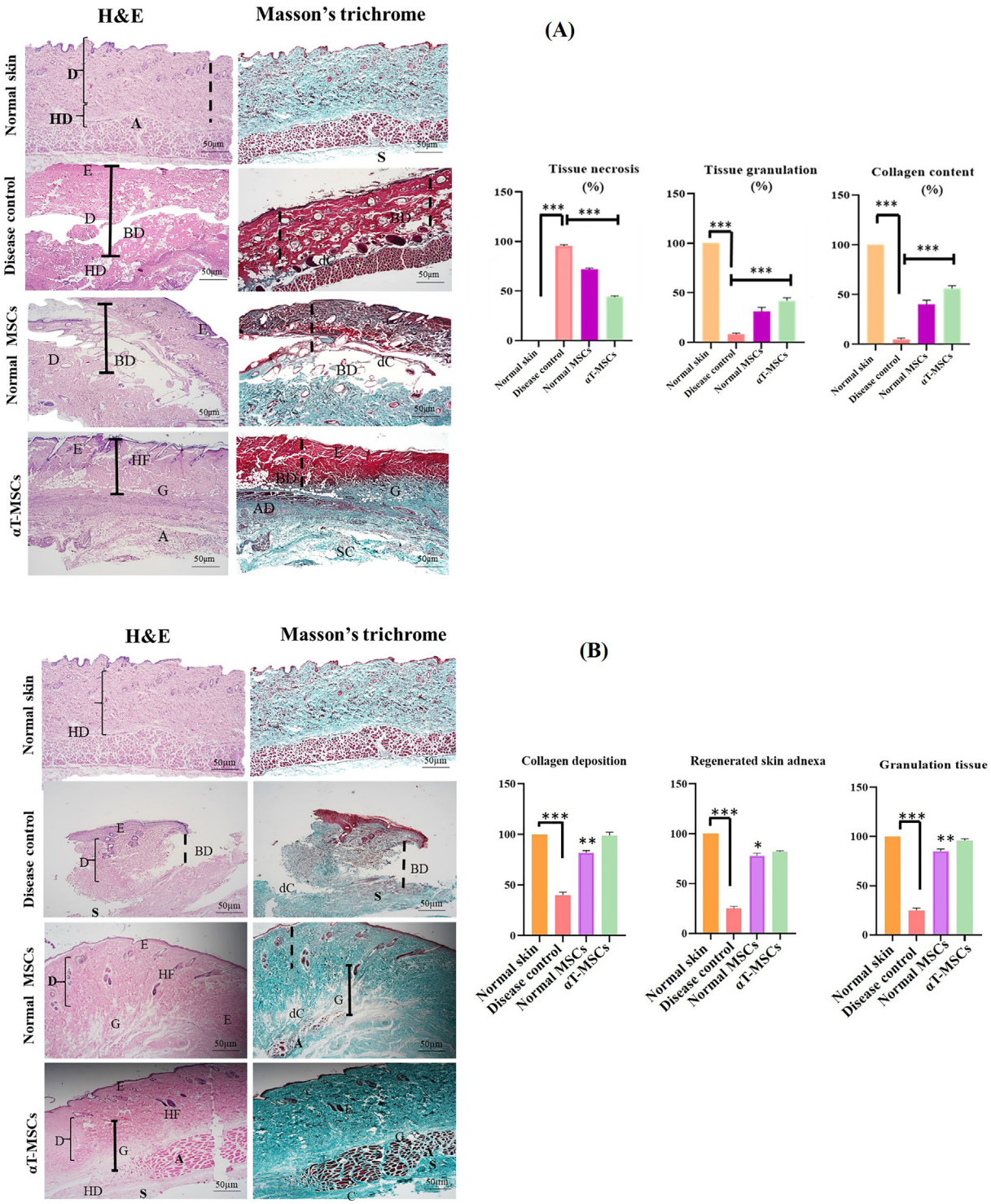


**Fig. 6.** Histological examination, scoring, and quantification. Bright field microscopic images show H & E and Masson's trichrome staining of normal skin and wound tissues at **(A)** early and **(B)** late phases of wound healing, scale bar = 50 μm. Group 2 revealed enhanced epidermal regeneration associated with tissue granulation and collagen fiber arrangement at the wound margin as compared to the other groups. Representative bar graphs and tables show quantification and scoring of histological parameters (tissue necrosis, collagen deposition, tissue granulation, and skin adnexa). For instance, tissue scoring (0–3; 0 = normal, 1 = mild, 2 = medium, and 3 = extensive) at corresponding time points (days 10, 40) and a final average score was given to each section after critical evaluation. E = epidermis, D = dermis, HD = hypodermis, BD = burn depth, HF = hair follicles, G = granulation tissue, A = adipose tissue, dC = damaged collagen, SC = subcutaneous tissue, AD = skin adnexa. One-way ANOVA with the Bonferroni post-hoc test was performed using IBM SPSS Statistic 21 software, and $p$-values ≤0.05 were considered statistically significant (*** = $p \leq 0.001$, ** = $p \leq 0.01$ and * = $p \leq 0.05$).

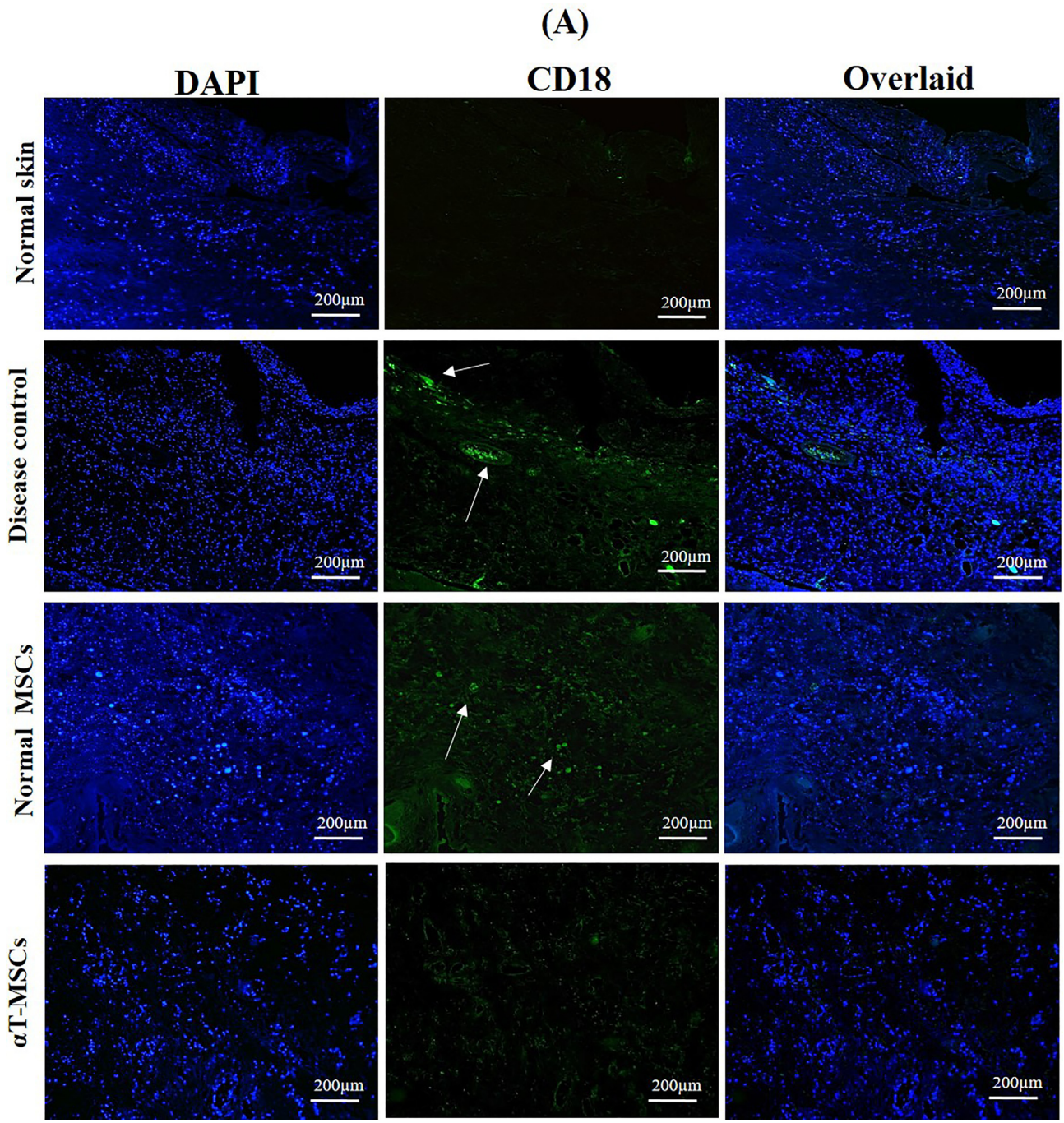


**Fig. 7.** Immunohistochemical expressions of CD18 and α-SMA at day 40. **(A)** CD18, a specific marker of leukocyte infiltration, was positively expressed in the control (disease) group and group 1, but not in the normal skin or group 2. **(B)** Positive expression of α-SMA shows enhanced formation of new blood vessels in both groups 1 and 2 as compared to control. **(C)** Quantitative analysis of CD18 and α-SMA in all experimental groups. One-way ANOVA with the Bonferroni post-hoc test was performed using IBM SPSS Statistic 21 software, and *p*-values ≤0.05 were considered statistically significant (*** = $p \leq 0.001$, ** = $p \leq 0.01$ and * = $p \leq 0.05$).

confirmed the role of αT-MSCs in suppressing the inflammation, thus mediating the wound healing process. It is consistent with our previous study wherein the antioxidant defense mechanism mediated by *PRDX-1* and *GPX-4* was observed to facilitate wound healing by effectively scavenging free radicals [17]. Apoptosis, a highly regulated cellular process, plays a crucial role in regulating various pathophysiological events by facilitating the elimination of unwanted cells. However, dysregulated or prolonged apoptosis may lead to fibrotic lesion that halts the healing process [39]. In this study, the apoptotic marker (*Bax*) was found to be downregulated in the αT-MSC group compared to the control and normal MSC treated groups. It may be attributed to the counteracting antioxidant defense mechanism, as indicated by elevated expression of *Bcl2*. Previous research has indicated that the activation of proapoptotic proteins such as *Bax* can be triggered by ROS production [40]. To conduct a comprehensive assessment of the wound healing

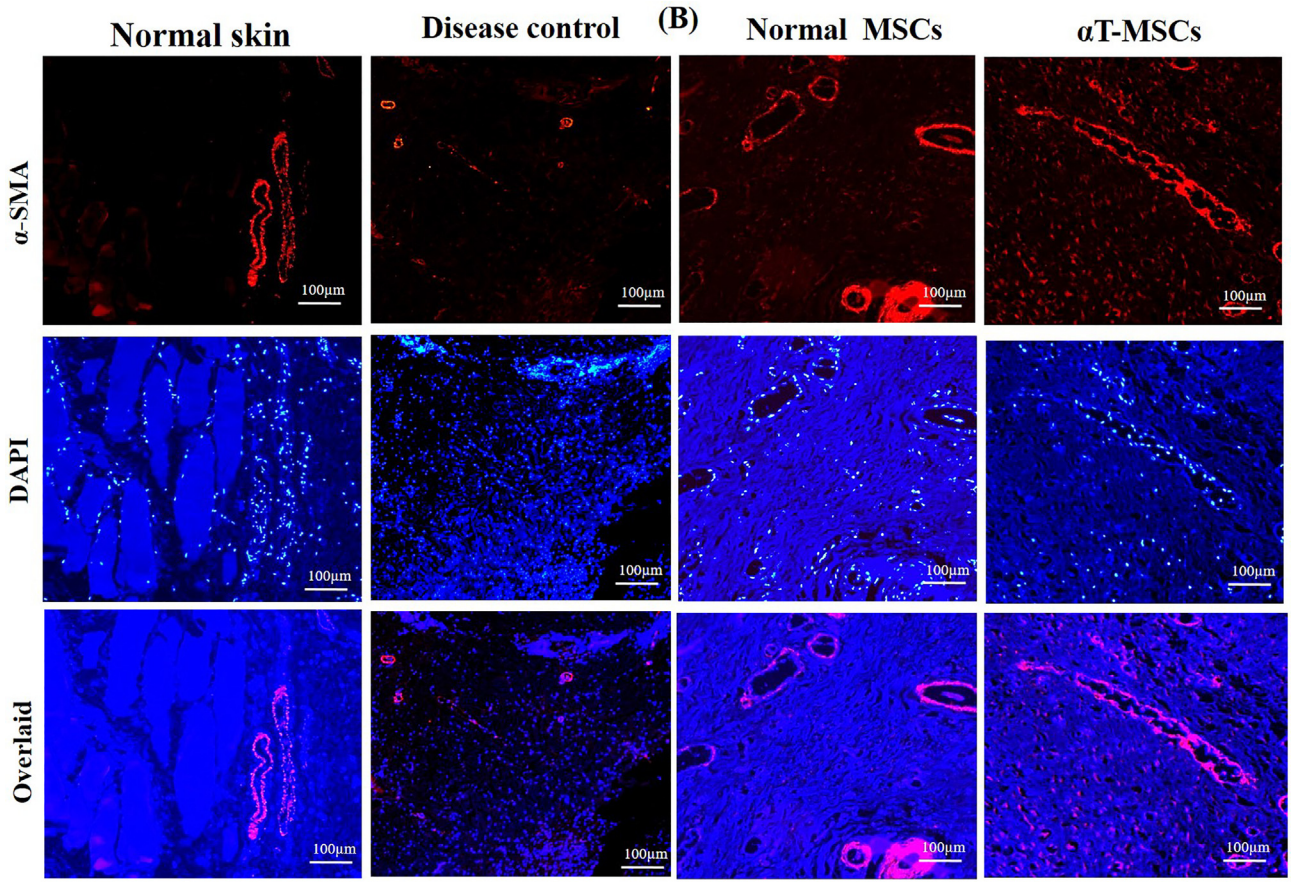


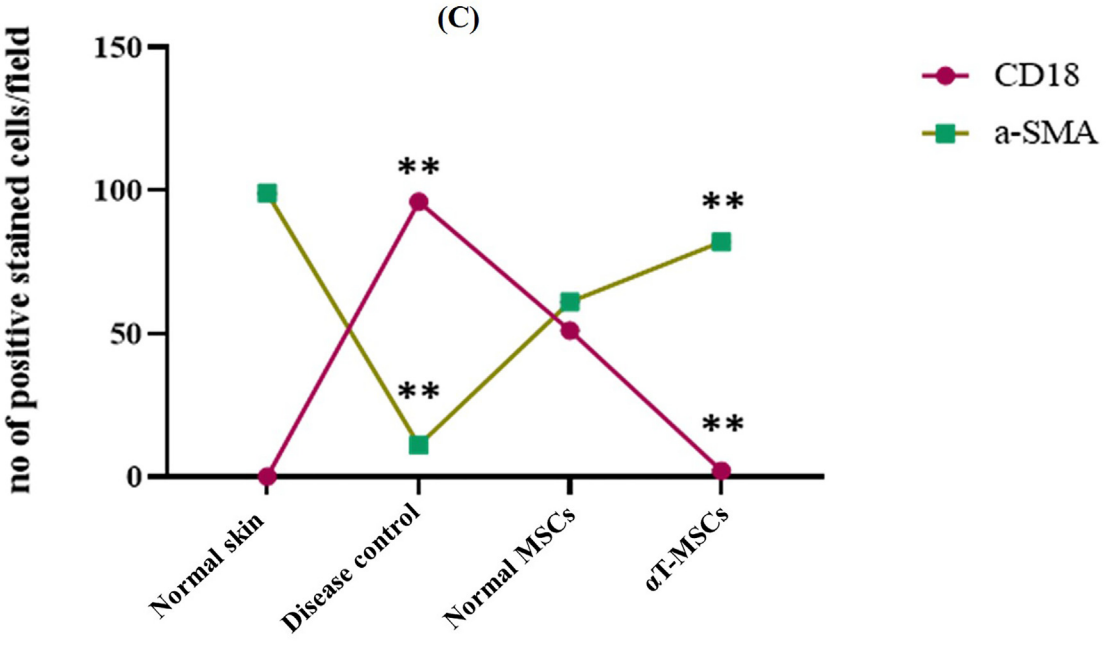


**Fig. 7.** (*continued*).

process, it is imperative to investigate the angiogenesis and tissue remodeling during the advanced stages of wound healing. Interestingly, αT-MSC treatment led to the upregulation of *VEGF, TGF-β, MMP-9, EGF, and PDGF* genes, representing enhanced neovascularization and re-epithelization. Collectively, recent advancements in the field of stem cell biology have increased the hope of achieving the definitive treatment for regenerative diseases which are considered incurable, such as diabetic foot ulcers, pressure ulcers, and other chronic long-standing conditions. It is important to understand the basic concepts of stem cell biology to utilize this technique effectively. Also, strategies to improve stem cell potential, e.g. preconditioning and tissue engineering

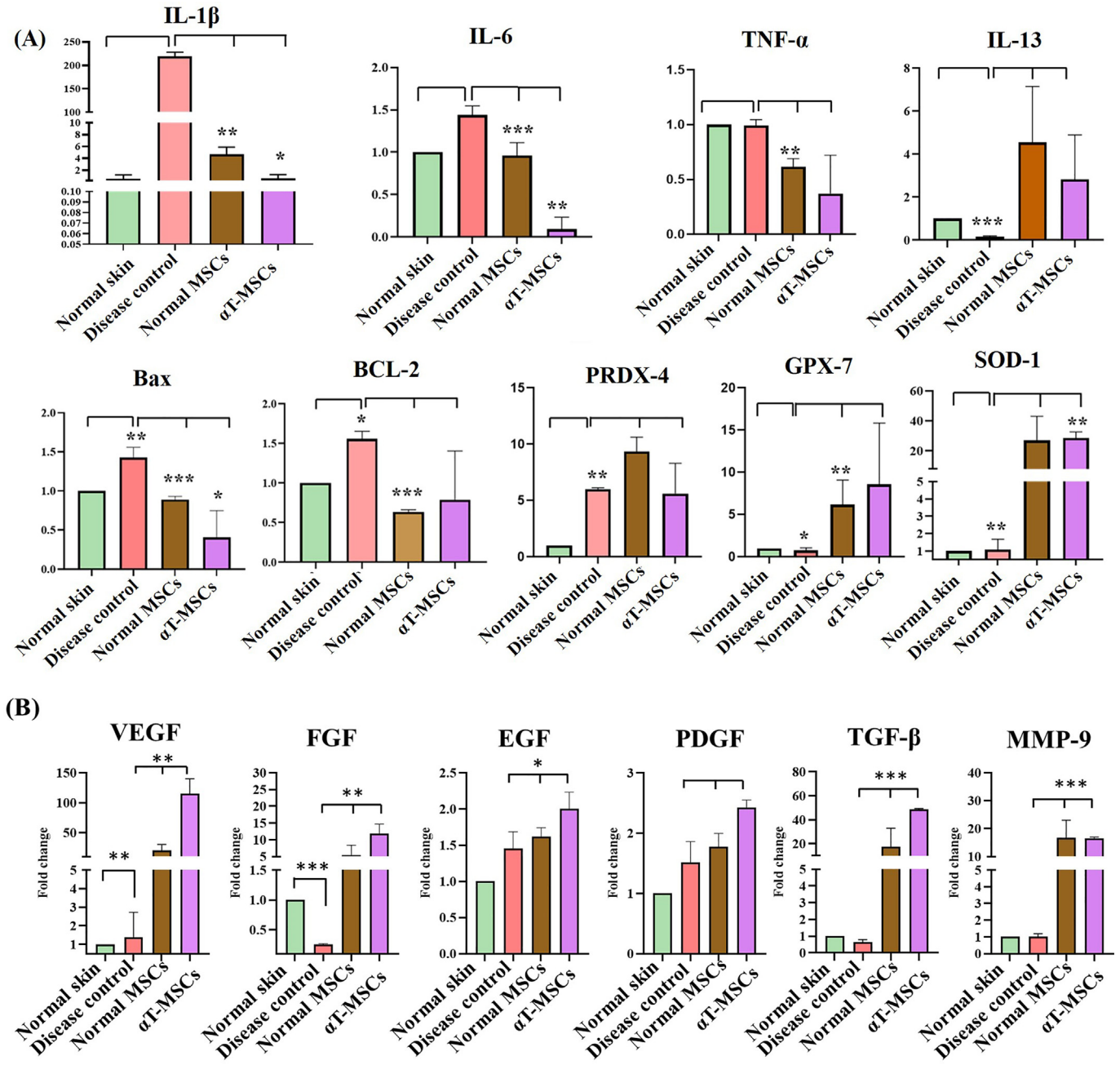


**Fig. 8.** Temporal change in the gene expression during wound healing phases. **(A)** Quantitative analysis of the reduced level of anti-inflammatory and increased level of anti-oxidative markers in both normal MSCs (group 1) and αT-MSCs (group 2) as compared to the control group at day 10. **(B)** Quantitative analysis of upregulation of pro/angiogenic and remodeling cytokines in both groups 1 and 2 as compared to the control group at day 40. One-way ANOVA with the Bonferroni post-hoc test was performed using IBM SPSS Statistic 21 software, and $p$-values $\leq 0.05$ were considered statistically significant (*** = $p \leq 0.001$, ** = $p \leq 0.01$ and * = $p \leq 0.05$).

approaches should be well understood. The data reported in this study has the potential to be useful for clinical practice after further optimization.

### 4.1. Clinical implication and limitations

Globally, burn wounds are more common skin injuries and require urgent attention of the healthcare system. Specialized facilities prioritize patient stabilization, infection prevention, and functional recovery. However, health workers frequently face difficulties that complicate patient stabilization during their recovery. In the current study, we examined the potential effect of a single dose of alpha terpineol preconditioned MSCs in chronic acid burn wounds. It is the first basic preclinical research showing comprehensive and successful regenerative potential of full thickness acid burn wounds. However, further investigation is required to elaborate these findings in higher species to mimic it's effects in humans, along with further safety analysis. Therefore, a better

**Table 2**
Scoring and quantification of histological parameters at day 10.

| Description | | Experimental groups | | | |
|---|---|---|---|---|---|
| S.no | Parameters | Normal skin | Disease control | Normal MSCs | αT-MSC |
| 1 | Burn depth (epidermal, dermal, dermal damages) | None, Intact layers | Damage extends to hypodermis | BD extends to dermis, but does not extend to the base of the hypodermis | BD extends beneath the hair bulbs, but not in the dermis |
| 2 | Tissue necrosis | none | completely necrosis ≥95% | deep ≥67% | partial ≥46% |
| 3 | Granulation tissue, Visual inspection, and absolute measure (mm) | no GT, normal intact dermis | no evidence of GT ≥ 8–10 % | thin GT, ≥32–38 % | Dermal layer intact no granular infiltrates consistent with healing ≥45% |
| 4 | Collagen deposition | 100% | 5–6% | 40–42% | 50–55% |
| 5 | Total scoring (0–3) 0-normal, 1-mild, 2- medium, 3-excessive | 0 | 3 | 2 | 2 |

**Table 3**
Scoring and quantification of histological parameters at day 40.

| Description | | Experimental groups | | | |
|---|---|---|---|---|---|
| S.no | Parameters | Normal skin | Disease control | Normal MSCs | αT-MSCs |
| 1 | Regeneration of skin layers | Intact layers | Damage extends to hypodermis with detachment of epidermis and dermis | Regeneration of epidermis and dermis with partially damage of hypodermis | Dermis intact with hypodermis, complete re-epithelialization |
| 2 | Granulation tissue, Visual inspection, and absolute measure (%) | no GT, normal intact dermis | Incomplete profile of GT ≥ 25% | Thick GT ≥ 82–90% | Complete GT ≥ 95% |
| 3 | Number of regenerated skin adnexa (hair follicles) per field | 100 | ≥20 | ≥78 | ≥82 |
| 4 | Collagen deposition | 100% | 40% | 82% | 98% |
| 5 | Total scoring (0–3) 0-normal, 1-mild, 2- medium, 3-excessive | 0 | 2 | 1 | 0 |

understanding is required to develop novel therapeutic approaches that target different pathways to reduce burn wound progression and enhance healing or wound closure.

## 5. Conclusion

The current study is the first study documenting a preclinical model of full thickness acid burn wounds. The study showed that MSCs have tremendous potential for the regeneration of chronic burn wounds. The characterized competencies of MSCs, along with their promising attributes of releasing anti-inflammatory and pro-angiogenic mediators, highlight their importance in the mechanism of wound healing. However, alpha terpineol preconditioned MSCs (αT-MSCs) remarkably enhanced the healing of acid burn wounds, mediated through their anti-inflammatory and anti-oxidative stress properties, and concurrently promoted neo-vascularization. Moreover, MSCs have great potential to migrate towards injury sites *in vivo* and modulate inflammation, promote tissue repair, and facilitate the angiogenesis process. It is expected that these outcomes could be used as a promising cellular therapeutic approach, serving as an alternative to skin grafting or plastic surgery, enabling the development of future clinical studies targeting chronic burn wounds. Further investigations may serve to validate this research and offer valuable perspectives on the clinical applications of these findings.

## Data availability

The authors have disclosed original data in this manuscript.

## Funding information

This study is financially supported by the National Research Program for Universities (NRPU-HEC) project under grant number 20-17590.

## Contribution

Fatima Jameel conducted all experiments with technical and analytical assistance from Irfan Khan. Fatima Jameel also wrote the first draft. Asmat Salim conceived the idea, critically analyzed the results, and wrote the manuscript in its final form. Fatima Irfan assisted *in vivo* experiments. Enam A. Khalil assisted with the technical guidance of experiments and helped in the writing of the manuscript.

## Declaration of competing interest

The authors have nothing to disclose.

## Acknowledgment

This study is financially supported by the National Research Program for Universities (NRPU-HEC) project under grant number 20-17590. Human umbilical cord samples were provided by the Zainab Panjwani Memorial Hospital after getting consent from donors.

## Appendix A. Supplementary data

Supplementary data to this article can be found online at https://doi.org/10.1016/j.reth.2024.05.008.

## References


[1] Baradaran-Rafii A, Eslani M, Haq Z, Shirzadeh E, Huvard MJ, Djalilian AR. Current and upcoming therapies for ocular surface chemical injuries. Ocul Surf 2017;15(1):48–64.
[2] Abbasi H, Dehghani A, Mohammadi AA, Ghadimi T, Keshavarzi A. The epidemiology of chemical burns among the patients referred to burn centers in shiraz, southern Iran, 2008–2018. Bulletin of Emergency Trauma 2021;9(4):195.
[3] Trief D, Chodosh J, Colby K, Griffiths D. Chemical (alkali and acid) injury of the conjunctiva and cornea. American Academy of Ophthalmology; 2017.
[4] Masterson A, Bleay S. The effect of corrosive substances on fingermark recovery: a pilot study. Sci Justice 2021;61(5):617–26.
[5] Muhammad G, Xu J, Bulte JW, Jablonska A, Walczak P, Janowski M. Transplanted adipose-derived stem cells can be short-lived yet accelerate healing of acid-burn skin wounds: a multimodal imaging study. Sci Rep 2017;7(1):1–11.
[6] Palao R, Monge I, Ruiz M, Barret JP. Chemical burns: pathophysiology and treatment. Burns 2010;36(3):295–304.
[7] Gnaneswaran N, Perera E, Perera M, Sawhney R. Cutaneous chemical burns assessment and early management. Aust Fam Physician 2015;44(3):135–9.
[8] Martin P, Nunan R. Cellular and molecular mechanisms of repair in acute and chronic wound healing. Br J Dermatol 2015;173(2):370–8.
[9] Oryan A, Alemzadeh E, Moshiri A. Burn wound healing: present concepts, treatment strategies, and future directions. J Wound Care 2017;26(1):5–19.
[10] Guillamat-Prats R. The role of MSC in wound healing, scarring, and regeneration. Cells 2021;10(7):1729.
[11] Patterson CW, Stark M, Sharma S, Mundinger GS. Regeneration and expansion of autologous full-thickness skin through a self-propagating autologous skin graft technology. Clinical case reports 2019;7(12):2449–55.
[12] Bay C, Chizmar Z, Reece EM, Yu JZ, Winocour J, Vorstenbosch J, Winocour S. Comparison of skin substitutes for acute and chronic wound management. In Seminars in Plastic Surgery35. New York, NY 10001, USA: Thieme Medical Publishers, Inc; 2021, August. p. 171–80.
[13] Al-Otaibi AM, Al-Gebaly AS, Almeer R, Albasher G, Al-Qahtani WS, Moneim AEA. Melatonin pre-treated bone marrow derived-mesenchymal stem cells prompt wound healing in rat models. Biomed Pharmacother 2022;145:112473.
[14] Li Z, Maitz P. Cell therapy for severe burn wound healing. Burns trauma 2018;6.
[15] Johnson LD, Pickard MR, Johnson WE. The comparative effects of mesenchymal stem cell transplantation therapy for spinal cord injury in humans and animal models: a systematic review and meta-analysis. Biology 2021;10(3):230.
[16] Zhang J, Qu X, Li J, Harada A, Hua Y, Yoshida N, Miyagawa S. Tissue sheet engineered using human umbilical cord-derived mesenchymal stem cells improves diabetic wound healing. Int J Mol Sci 2022;23(20):12697.
[17] Irfan F, Jameel F, Khan I, Aslam R, Faizi S, Salim A. Role of quercetin and rutin in enhancing the therapeutic potential of mesenchymal stem cells for cold induced burn wound. Regenerative Therapy 2022;21:225–38.
[18] Guo L, Du J, Yuan DF, Zhang Y, Zhang S, Zhang HC, Huang H. Optimal H2O2 preconditioning to improve bone marrow mesenchymal stem cells' engraftment in wound healing. Stem Cell Res Ther 2020;11(1):1–17.
[19] Ma C, Sun Y, Pi C, Wang H, Sun H, Yu X, He X. Sirt3 attenuates oxidative stress damage and rescues cellular senescence in rat bone marrow mesenchymal stem cells by targeting superoxide dismutase 2. Front Cell Dev Biol 2020;8:599376.
[20] Li Y, Liu D, Tan F, Yin W, Li Z. Umbilical cord derived mesenchymal stem cell-GelMA microspheres for accelerated wound healing. Biomed Mater 2022;18(1):015019.
[21] Aslam S, Khan I, Jameel F, Zaidi MB, Salim A. Umbilical cord-derived mesenchymal stem cells preconditioned with isorhamnetin: potential therapy for burn wounds. World J Stem Cell 2020;12(12):1652–66.
[22] Ahmed R, Afreen A, Tariq M, Zahid AA, Masoud MS, Ahmed M, Hasan A. Bone marrow mesenchymal stem cells preconditioned with nitric-oxide-releasing chitosan/PVA hydrogel accelerate diabetic wound healing in rabbits. Biomed Mater 2021;16(3):035014.
[23] Barreto RS, Albuquerque-Júnior RL, Araújo AA, Almeida JR, Santos MR, Barreto AS, Quintans-Júnior LJ. A systematic review of the wound-healing effects of monoterpenes and iridoid derivatives. Molecules 2014;19(1):846–62.
[24] Wu XL, Liou CJ, Li ZY, Lai XY, Fang LW, Huang WC. Sesamol suppresses the inflammatory response by inhibiting NF-κB/MAPK activation and upregulating AMP kinase signaling in RAW 264.7 macrophages. Inflamm Res 2015;64:577–88.
[25] Costa MF, Durço AO, Rabelo TK, Barreto RDSS, Guimarães AG. Effects of Carvacrol, Thymol and essential oils containing such monoterpenes on wound healing: a systematic review. J Pharm Pharmacol 2019;71(2):141–55.
[26] Mirza A, Khan I, Salim A, Husain M, Herzig JW. Role of Wnt/β-catenin pathway in cardiac lineage commitment of human umbilical cord mesenchymal stem cells by zebularine and 2'-deoxycytidine. Tissue Cell 2022;77:101850.
[27] Ishaque A, Khan I, Salim A, Malick TS, Adli DSH. Effect of α-pinene and thymoquinone on the differentiation of bone marrow mesenchymal stem cells into neuroprogenitor cells. Bioimpacts: BI 2022;12(2):147.
[28] Zhao Y, Wang M, Liang F, Li J. Recent strategies for enhancing the therapeutic efficacy of stem cells in wound healing. Stem Cell Res Ther 2021;12(1):1–18.
[29] Masaki S, Maeda I, Kawamoto T. Conservative management of full-thickness burn wounds using advanced moist dressings: a case report. Wounds: a Compendium of Clinical Research Practice 2022;34(6):E42–6.
[30] Hu MS, Borrelli MR, Lorenz HP, Longaker MT, Wan DC. Mesenchymal stromal cells and cutaneous wound healing: a comprehensive review of the background, role, and therapeutic potential. Stem Cell Int 2018:1–13. https://doi.org/10.1155/2018/6901983 [PMID: 29887893.
[31] Jeschke MG, Rehou S, McCann MR, Shahrokhi S. Allogeneic mesenchymal stem cells for treatment of severe burn injury. Stem Cell Res Ther 2019;10:1–6.
[32] Demilew W, Adinew GM, Asrade S. Evaluation of the wound healing activity of the crude extract of leaves of Acanthus polystachyus Delile (Acanthaceae). Evid base Compl Alternative Med 2018:1–9.
[33] Guo HF, Ali RM, Abd Hamid R, Chang SK, Zainal Z, Khaza'ai H. A new histological score grade for deep partial-thickness burn wound healing process. International journal of burns trauma 2020;10(5):218.
[34] Wang M, Xu X, Lei X, Tan J, Xie H. Mesenchymal stem cell-based therapy for burn wound healing. Burns trauma 2021;9:tkab002.
[35] Vyas KS, Vasconez HC. Wound healing: biologics, skin substitutes, biomembranes and scaffolds. Healthcare 2014;2(3).
[36] Stupin V, Manturova N, Silina E, Litvitskiy P, Vasin V, Artyushkova E, Aliev S. The effect of inflammation on the healing process of acute skin wounds under the treatment of wounds with injections in rats. J Exp Pharmacol 2020:409–22.
[37] Karim AS, Liu A, Lin C, Uselmann AJ, Eliceiri KW, Brown ME, Gibson AL. Evolution of ischemia and neovascularization in a murine model of full thickness human wound healing. Wound Repair Regen 2020;28(6):812–22.
[38] Coentro JQ, Pugliese E, Hanley G, Raghunath M, Zeugolis DI. Current and upcoming therapies to modulate skin scarring and fibrosis. Adv Drug Deliv Rev 2019;146:37–59.
[39] Cheng P, Li S, Chen H. Macrophages in lung injury, repair, and fibrosis. Cells 2021;10(2):436.
[40] Arya AK, Tripathi R, Kumar S, Tripathi K. Recent advances on the association of apoptosis in chronic non healing diabetic wound. World J Diabetes 2014;5(6):756.